CHAPTER SEVEN

Electrocatalytic Detection of Dopamine at Single-Walled Carbon Nanotubes-Iron (iii) Oxide Nanoparticles Platform*

* The following publications resulted from part of the research work presented in this chapter and are not referenced further in this thesis:

7. **Abolanle S. Adekunle**, Bolade O. Agboola, Jeseelan. Pillay, Kenneth I. Ozoemena, *Sens. Actuator: Chemical B*, 148 (2010) 93-102.
8. **Abolanle S. Adekunle**, Kenneth I. Ozoemena, *Int. J. Electrochem. Sci.* (in press).

7.1. Characterisation with FESEM, AFM, EDX and XPS

FESEM images of typical modification steps are summarised in scheme 7.1. There is a clear evidence of edge-plane sites uniformly distributed on the bare-EPPGE. The electrode is covered with SWCNT after modification with the acid-treated SWCNT on the bare EPPGE (EPPGE-SWCNT).

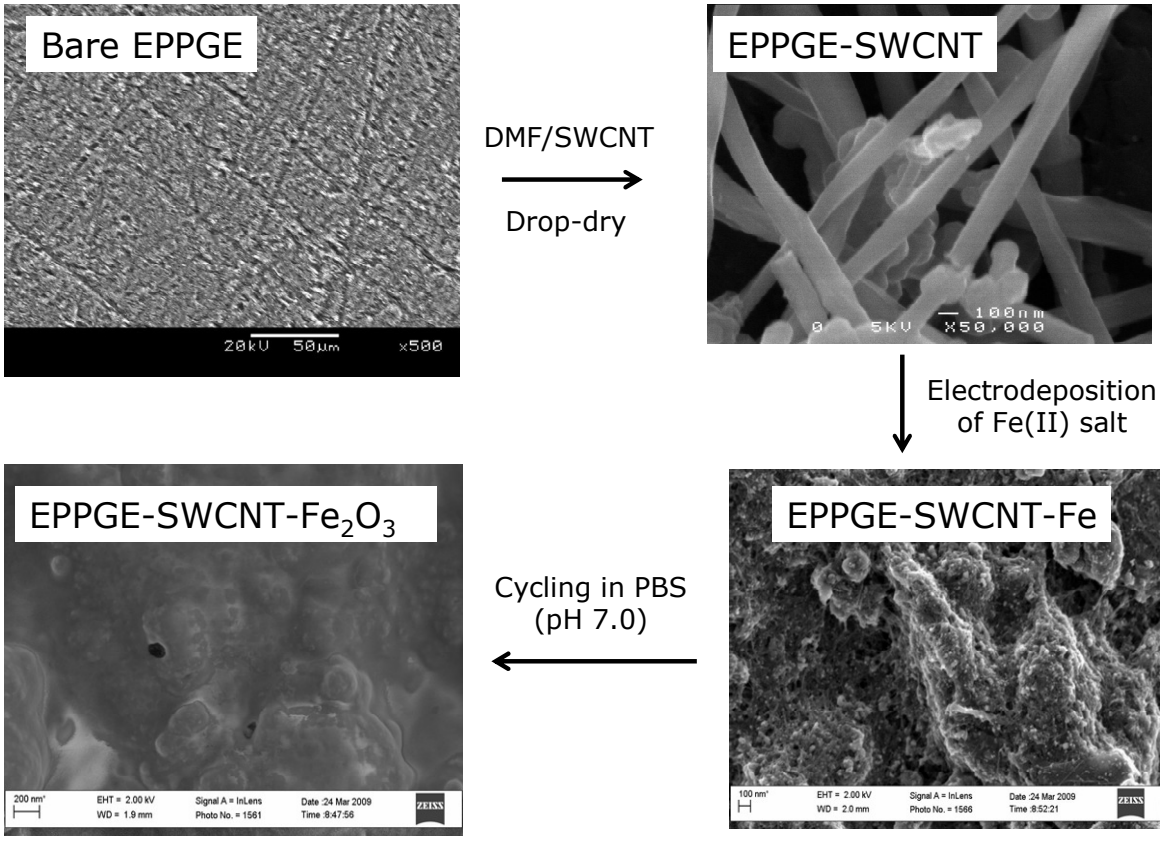

Scheme 7.1: Schematic of electrode modification process.

The ease of dispersion of the SWCNT suspension on the EPPGE bare electrode may be attributed to the strong π-π interaction between EPPGE and SWCNT. Electro-deposition of Fe particles on the EPPGE-SWCNT gave EPPGE-SWCNT-Fe. There is high dispersion of a

network of Fe nanoparticles that completely cover the SWCNT layer. This could be made possible because of the strong electrostatic interactions between the Fe^{2+} ions in solution and the COO^- of SWCNT on the electrode. After treating EPPGE-SWCNT-Fe electrode in aqueous PBS, pH 7.0, an EPPGE-SWCNT-Fe_2O_3 electrode was obtained. There is a clear transformation of the iron nanoparticles to iron oxides, mainly Fe_2O_3 as proved by XPS.

The AFM topography images (Figure 7.1) show similar surface morphology, which can be explained in the same manner as that given for the SEM images. It is much easier to view the particle distribution on the bare glassy carbon plate, SWCNT, SWCNT-Fe and SWCNT/Fe_2O_3 in nano sizes from the AFM images. From the cross section profile of the different modified electrodes (Figure 7.1), it could be observed that while the surface thickness of the bare plate are between 6–7 nm, the SWCNT paste are in the magnitude of 25 nm while the Fe and Fe_2O_3 particles are in the order of about 30 nm, indicating successful deposition and growth of nanoparticles on the electrode.

The EDX profile (Figure 7.2) gives insights into the elemental compositions of the modified electrodes. Bare EPPGE (a) predominantly showed carbon (~ 100%) which is an indication of a clean, unmodified electrode. The acid-treated SWCNT (b) confirmed presence of sulfur peak and oxo-functionality (presence of oxygen peak), attributed to the treatment of the SWCNT with sulfuric acid solution and its subsequent washing with copious amount of water. The metal impurities especially nickel is characteristic of Aldrich SWCNT used in this study and cannot be completely removed during acid treatment.

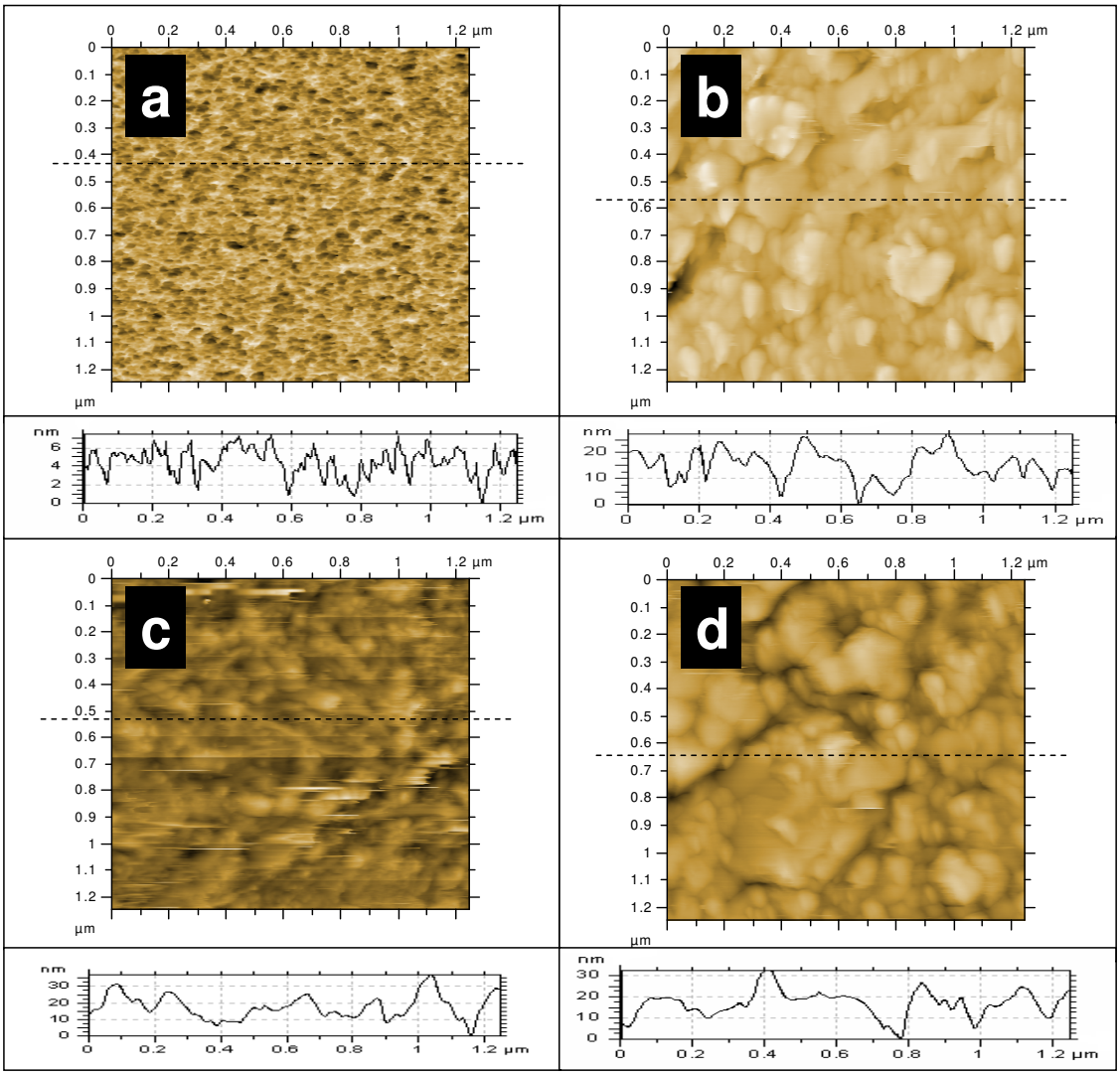

Figure 7.1: Typical AFM images of (a) bare glassy carbon (GC) plate, (b) GC-SWCNT, (c) SWCNT-SWCNT-Fe and (d) GCE-SWCNT-Fe_2O_3.

EDX profile of c and d shows the presence of iron peaks which is a proof for the successful modification of EPPGE-SWCNT-Fe (c) and EPPGE-SWCNT-Fe_2O_3 (d) with iron nanoparticles. The P and Na peaks in the EDX of EPPGE-SWCNT-Fe_2O_3 arise from the sodium phosphate

salt used for the electrolyte while the enhanced oxygen peak confirms the modification of the electrode to its oxide form.

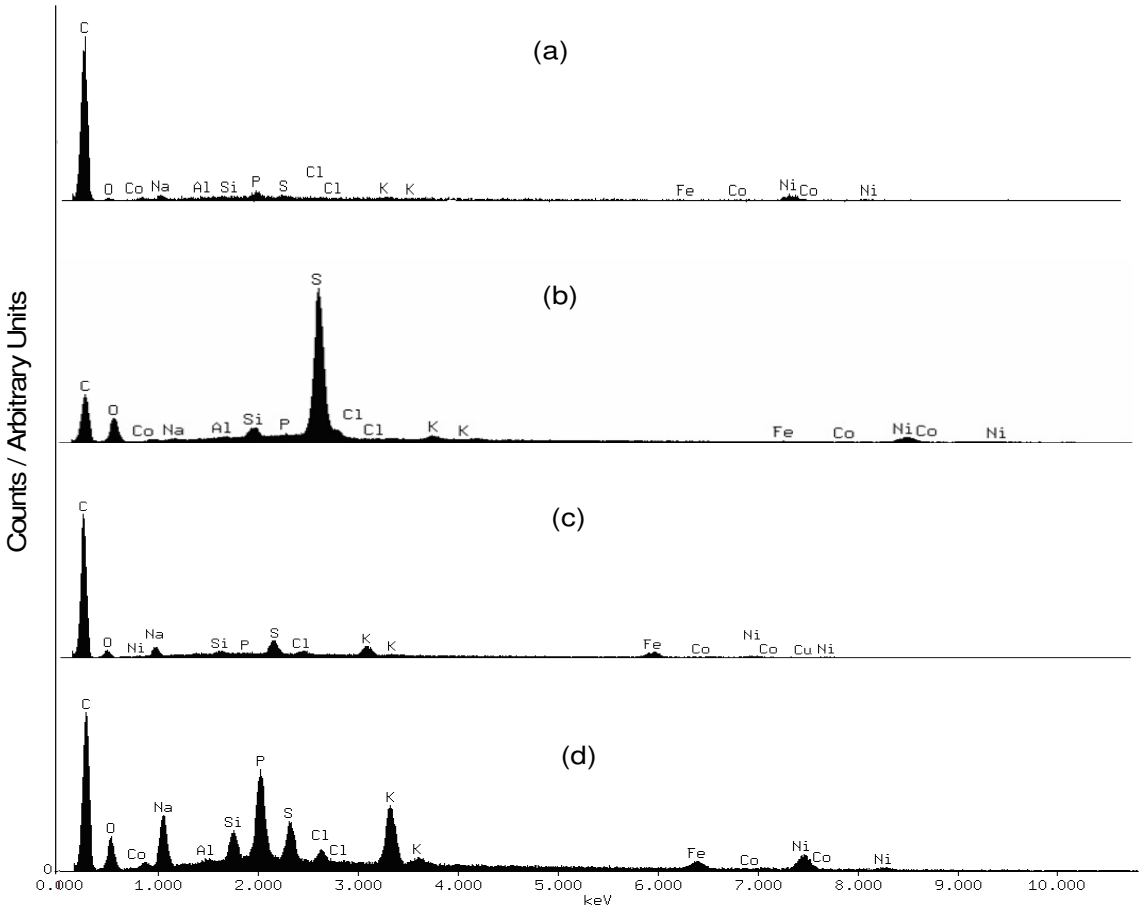

Figure 7.2: Typical EDX profile of the (a) bare EPPGE, (b) EPPGE-SWCNT, (c) EPPGE-SWCNT-Fe and (d) EPPGE-SWCNT-Fe_2O_3.

Figure 7.3 presents the XPS results of the EPPGE-SWCNT-Fe_2O_3 modified electrode in 0.1 M pH 7.0 PBS. XPS data analysis was aimed at determining quantitatively the relative amounts of the two chemical species of Fe, which are Fe^{2+} and Fe^{3+} in the recorded spectrum. The Fe $2p_{3/2}$ peak at 713.6 eV (enlarged in the inset, Figure 7.3) agreed with literature value of 711.0 eV which indicates the presence of Fe_2O_3 species [1,2]. The weak peak at 727.2 eV

corresponding to Fe $2p_{1/2,}$ agreed closely with 724.6 eV reported in literature [2], associated with Fe_3O_4 species. The sharp nature of the O1s peak (532 eV) also suggests that the oxygen is in one oxidation state. The O1s peak is very close to the 530 eV reported to be the lattice oxygen of Fe_2O_3 and Fe_3O_4 [2,3]. The dominant oxide of Fe on modified electrode from this result can be taken as Fe_2O_3 since species of Fe_3O_4 are not apparent. The Na and the P peaks in Figure 7.3 can be attributed to the Na and P of the PBS used during electrode modification while the C peak can be attributed to the carbon of the SWCNT and the base EPPGE electrode.

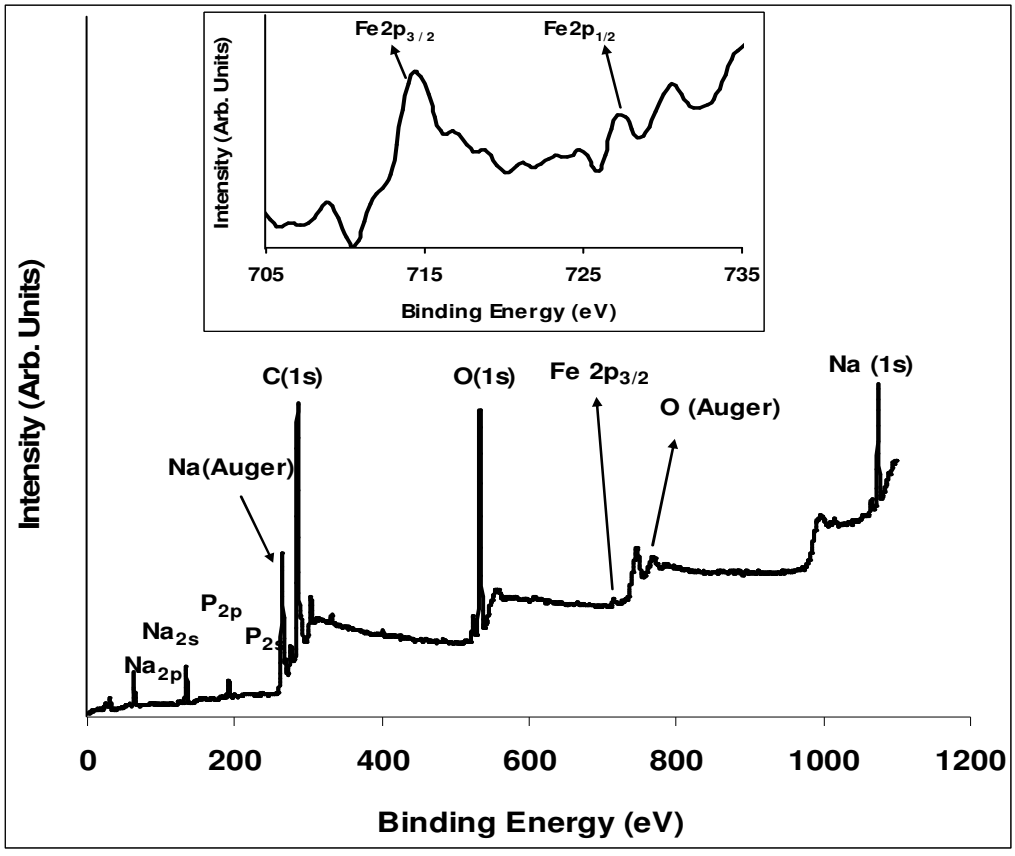

Figure 7.3: Typical XPS of EPPGE-SWCNT-Fe_2O_3 modified electrode. Inset shows the enlarged portion showing the peak corresponding to the Fe $2p_{3/2}$ and Fe $2p_{1/2}$ bands.

7.2. Electrocatalytic detection of dopamine: Voltammetric and Impedimetric properties

Figure 7.4 compares the cyclic voltammograms, original (a) and background-subtracted (b) of bare EPPGE (i), EPPGE-SWCNT (ii), EPPGE-SWCNT-Fe (iii), and EPPGE-SWCNT-Fe_2O_3 (iv) in 0.1 M PBS (pH 7.0) containing 2 x 10^{-4} M dopamine (DA). As easily seen from the original voltammograms, the electrodes containing SWCNT are associated with large background (capacitive) current responses, characteristic of acid-treated SWCNT [4]. DA redox couple at $E_{1/2}$ of *ca* 0.2 V is due to Dopamine / Quinone redox process. The current response of each electrode after the subtraction of the buffer current follow this trend: EPPGE-SWCNT-Fe_2O_3 (~ 50.45 µA) > EPPGE-SWCNT (~ 23.24 µA) and EPPGE-SWCNT-Fe (~ 22.80 µA), bare EPPGE (~ 6.62 µA), indicating the enhanced response of the EPPGE-SWCNT-Fe_2O_3 compared to other electrodes.

Next, the electron transfer properties of the four electrodes towards the voltammetric detection of dopamine using the EIS strategy were investgated. EIS is a powerful non-destructive and very informative technique for probing molecules at surfaces. It provides vital information about the charge transfer phenomenon across the electrode|electrolyte interface [5-7]. Figure 7.5a shows the impedance spectra (Nyquist plots) obtained for the electrodes, EPPGE (i), EPPEGE-SWCNT (ii), EPPGE-SWCNT-Fe (iii) and EPPGE-SWCNT-Fe_2O_3 (iv) in 2 x 10^{-4} M DA solution performed at a fixed potential (0.2 V vs. Ag|AgCl sat'd KCl) and frequencies between 10 kHz and 0.1 Hz. The choice of the fixed potential was based on the formal potential, $E_{1/2}$, of the DA which is the sum of the values of the anodic and the cathodic peak potential divided by two (i.e., $(E_{pa}+E_{pc})/2$). The experimental data were successfully fitted with the

Randles circuit model (Figure 7.5b) where the element R_s, R_{ct}, C_{dl} and Z_w are already defined. The parameters were fitted with satisfactory results (Table 7.1).

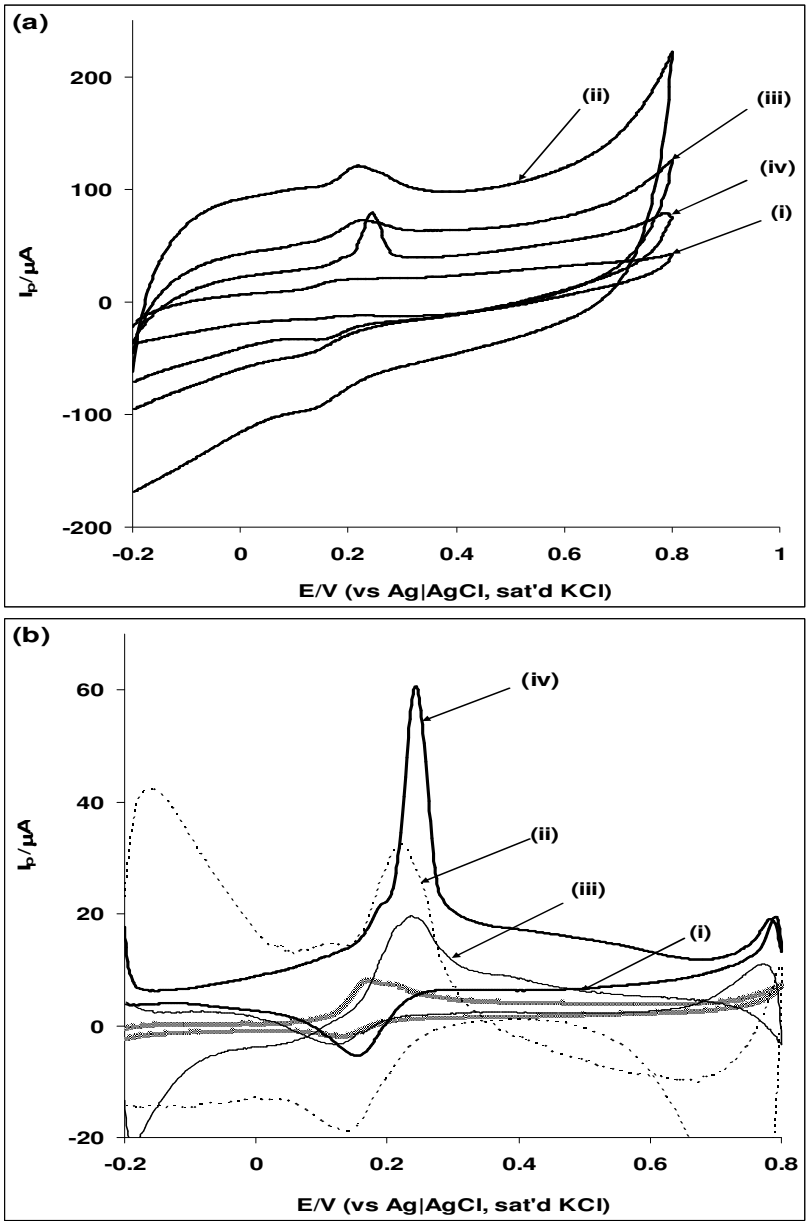

Figure 7.4: Typical cyclic voltammograms, original (a) and background- subtracted (b) of bare EPPGE (i), EPPGE-SWCNT (ii), EPPGE-SWCNT-Fe (iii), and EPPGE-SWCNT-Fe_2O_3 (iv) in 0.1 M PBS (pH 7.0) containing 2 x 10^{-4} M DA (Scan rate = 25 mV s^{-1}).

EPPGE-SWCNT-Fe_2O_3 has the lowest R_{ct} value (1.29 Ωcm^2) compared with the bare EPPGE (16.20 Ωcm^2), EPPGE-SWCNT (1.68 Ωcm^2) and the EPPGE-SWCNT-Fe (1.92 Ωcm^2) electrodes. Note that the C_{dl} is treated here as a constant phase element, CPE (a real application situation) rather than the ideal double layer capacitance [8, 9].

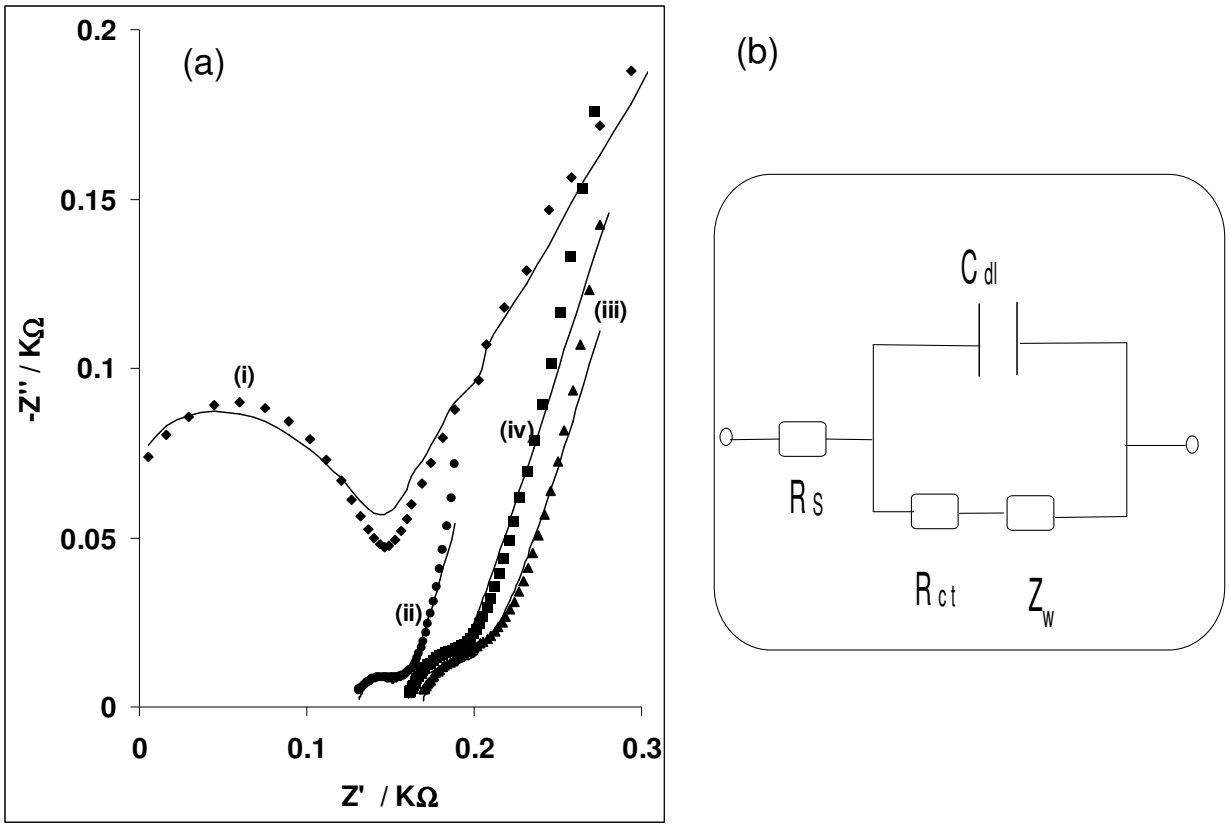

Figure 7.5: (a) Typical Nyquist plot of the bare EPPGE (i), EPPGE-SWCNT (ii), EPPGE-SWCNT-Fe (iii), and EPPGE-SWCNT-Fe_2O_3 (iv) obtained in 0.1 M PBS containing 2 x 10^{-4} M DA (biased at 0.2 V), between 10 KHz and 0.1 Hz, and (b) Equivalent circuit model used in fitting the spectra obtained in Figure 7.5 (a).

Table 7.1: Impedance data obtained for the electrodes in 2 x 10^{-4} M DA solution in pH 7.0 PBS (at 0.2 V vs Ag|AgCl sat'd KCl).

Electrodes	Electrochemical impedance spectroscopy data				
	$R_s/\Omega\ cm^2$	$C_{dl}/\mu F cm^{-2}$	$R_{ct}/\Omega cm^2$	$Z_W/\Omega\ cm^2$	k_s/cms^{-1}
EPPGE	-4.34±0.04	1.42±0.06	16.20±0.03	30.54±0.04	0.02±0.03
EPPGE-SWCNT	13.13±0.01	76.30±14.93	1.68±0.02	522.00±1.72	0.20±0.02
BPPGE-SWCNT-Fe	16.94±0.02	80.7±18.75	1.92±0.02	255.00±0.71	0.17±0.02
BPPGE-SWCNT-Fe_2O_3	15.88±0.04	53.3±11.56	1.29±0.04	193.80±0.72	0.26±0.04

The electron transfer rate constants (k_s) may be obtained from the R_{ct} values from the derived Equations (7.1-7.3) [10, 11].

$$R_{ct} = \frac{RT}{nFi_o} \tag{7.1}$$

$$i_o = nFAk_s C_O^{\infty} C_R^{\infty} \tag{7.2}$$

Combining Equations 7.1 and 7.2, taking the activity coefficients (∞) equal to unity, and assuming the bulk concentrations of the oxidized and reduced species to be equal ($C_O^{\infty} = C_R^{\infty} = C$) such that the equilibrium potential ($E_{1/2}$) equals the formal redox potential ($E_{O/R}^{\phi}$), then the k_s becomes:

$$k_s = \frac{RT}{n^2 F^2 A R_{ct} C} \tag{7.3}$$

where n = 2, *A* is the area of the electrode, C is the concentrations of (mol cm^{-3}) of dopamine, R, T and F have their usual meanings. The k_s value decreases as follows: EPPGE-SWCNT-Fe_2O_3 (~ 0.26 cms^{-1}) > EPPGE-SWCNT (~ 0.20 cms^{-1}) > EPPGE-SWCNT-Fe (~ 0.17 cms^{-1})> bare EPPGE (~ 0.02 cms^{-1}). The high k_s value of the EPPGE-SWCNT-Fe_2O_3 indicates faster electron transfer response towards the electrocatalysis of DA. Both CV and EIS data prove that the EPPGE-SWCNT-Fe_2O_3 hybrid exhibit better response towards the electrochemistry of DA compared to the other electrodes studied in this work. CNTs are known to enhance electrocatalytic response [12, 13]. Thus, these results could be associated with a combination of factors, such as the synergistic behaviour between the high electron-

conducting CNTs and the affinity between Fe^{3+} and DA [14], the ease of diffusion of the DA through the porous-like SWCNT-Fe_2O_3 film to the catalytic sites of the electrode, the larger available surface area of the modified electrode due to the nanometric dimension of the nanotubes and, finally the strong combination tendency of SWCNT-Fe_2O_3 to DA by electrostatic interaction. The last point can be substantiated by looking at the ionic form of DA in PBS. DA is positively charged at pH under 7.4 or in neutral environment [15]. This is due to the protonation of the nitrogen atom on the molecule. Hence, while the EPPGE-SWCNT-Fe electrodes will attract DA with weaker force as a result of repulsion between like charges, it becomes easier for DA to be attracted towards the EPPGE-SWCNT-Fe_2O_3 film because of the electron-rich oxygen atom. This phenomenon may explain why the detection and catalysis of DA was much favoured at the EPPGE-SWCNT-Fe_2O_3 compared to other electrodes. Aside the fact that Fe is in its most stable oxidation state of +3 (Fe^{3+}) in the electrolyte, which makes it a strong catalyst and oxidant, it has also been reported that Fe^{3+} is chelated by the dihydroxy catechol group of dopamine, catechol, 5, 6-dihydroxyindole etc [14]. A report demonstrated that 7(2-aminoethyl)-3,4-dihydro-5-hydroxy-2H-1,4-benzothiazine-3 carboxylic acid (DHBT-1), containing –OH phenolic and >NH in six ring, had an ability of binding Fe^{3+} like 5, 6-dihydroxyindole [16]. It can therefore be concluded from these previous reports that the EPPGE-SWCNT-Fe_2O_3 modified electrode could be the best electrode towards DA oxidation based on the ability of Fe^{3+} to bind and form chelate with DA [14] and its oxidation intermediates. All other studies carried out in this work, unless otherwise stated, were focused on EPPGE-SWCNT-Fe_2O_3 electrode.

7.3. Effect of varying potential scan rates

Effect of potential scan rate (ν) was investigated by carrying out cyclic voltammetry experiment at constant concentration ($2x10^{-4}$ M) of the DA in 0.1 M PBS using the EPPGE-SWCNT-Fe_2O_3 electrode (Figure 7.6a). At a potential scan rate of 25 mVs^{-1}, a pair of well defined redox peaks, equilibrium potential ($E_{1/2}$) of 165 mV, a ratio of anodic to cathodic peak current (I_{pa} / I_{pc}) approximately 1.3 (slightly higher than the unit value expected for an ideal voltammetric reversibility), and a peak-to-peak separation (ΔE_p) of ~70 mV (slightly higher than the 59.8 mV value expected for a one-electron reversible process) was observed. The CV data indicate a quasi-reversible electro-oxidation of DA. The ΔE_p increases at higher potential scan rates. This slight deviation from ideality may be due to chemical interaction between DA and the film. It was observed that DA anodic and cathodic peaks increase simultaneously with increase in scan rates (scan rates ranged from 25–1000 mVs^{-1}). As in Figure 7.4, the anodic current is more pronounced than the reduction current, suggesting that the potential sweep favours electro oxidation of DA. This observed non-symmetrical forward and reverse peaks of DA in 0.1 M PBS (pH 7.0) should perhaps not be surprising as other workers [17] have also observed the same and ascribed it to the working pH conditions. At pH 5, the peaks are symmetrical but with increase in pH, the cathodic (reverse) peak significantly decreased. The plots of peak current, I_p for both anodic and cathodic versus square root of scan rate ($\nu^{1/2}$) (Figure 7.6b) were linear (R^2 = 0.9956 and 0.9939), signifying a diffusion-controlled redox process [18-21].

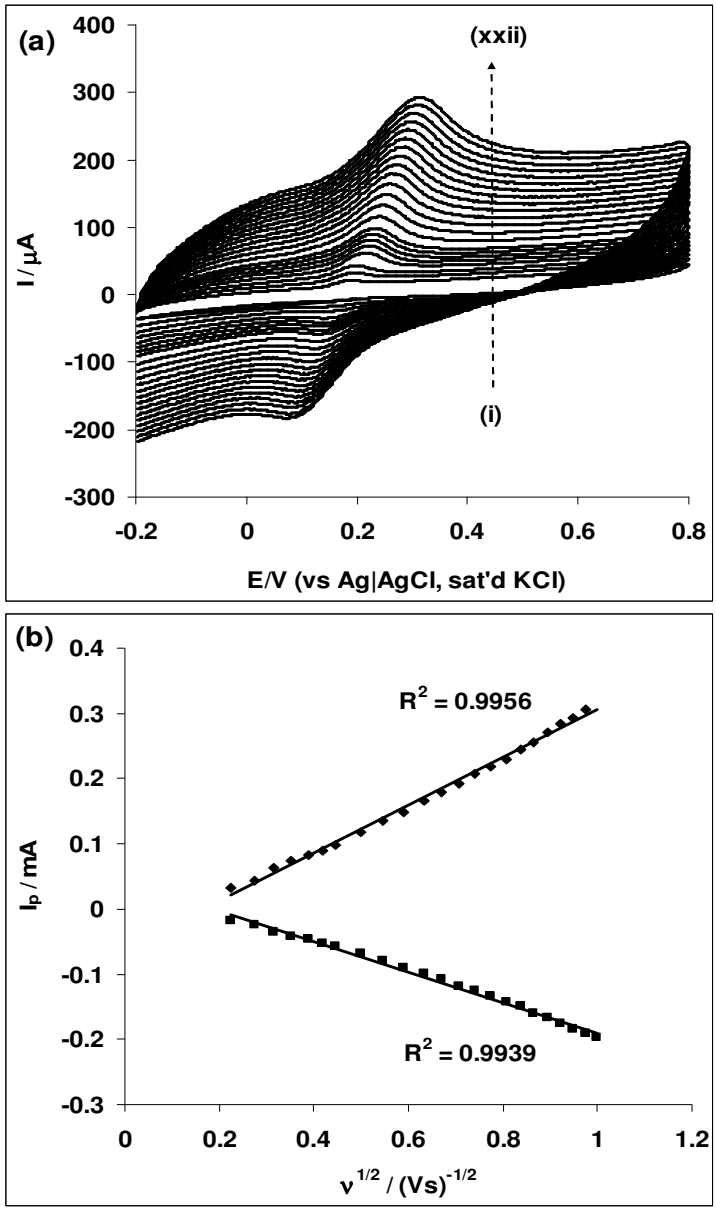

Figure 7.6: (a) Cyclic voltammetric evolutions of EPPGE-SWCNT-Fe_2O_3 obtained in 0.1 M PBS containing 2 x 10^{-4} M DA at scan rates 25 to 1000 mV s^{-1} (inner to outer). (b) Plot of I_p vs. $\nu^{1/2}$ for both anodic and cathodic process.

7.4. Analytical Application

Concentration study was carried out by investigating the response of EPPGE-SWCNT-Fe_2O_3 electrode to the different concentrations of DA (Figure 7.7) using square wave voltammetry (SWV). At DA concentration greater than 32 µM, the current response did not increase any further, a phenomenon usually attributed to the saturation of the catalytic sites.

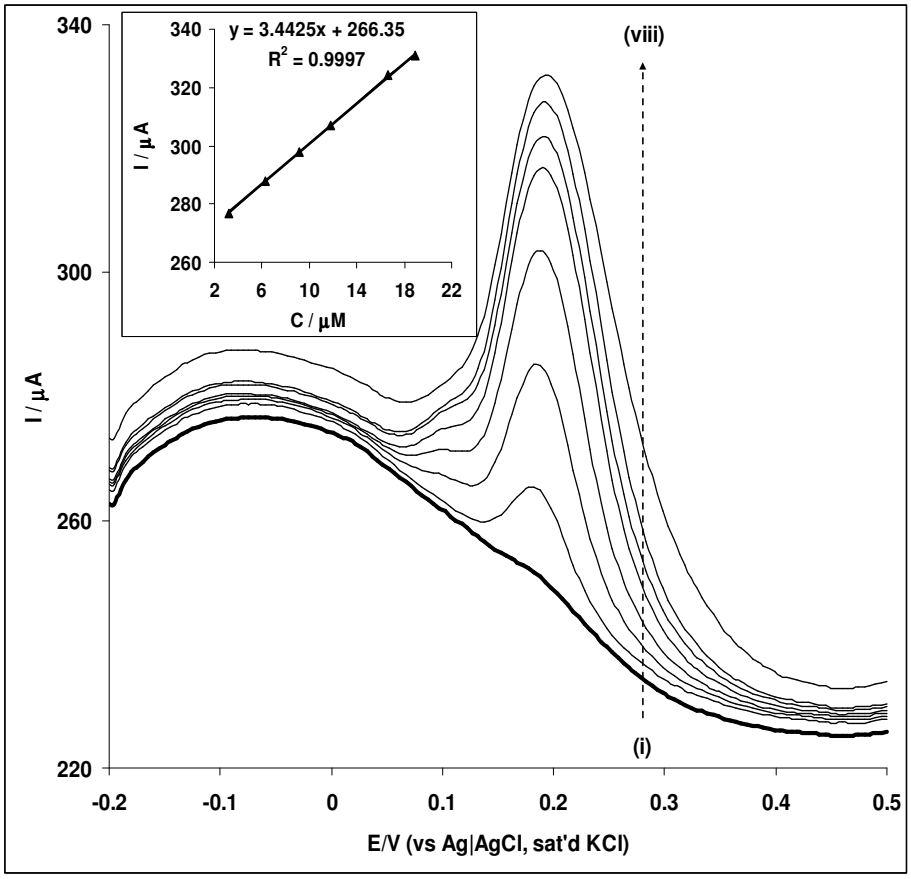

Figure 7.7: Square wave voltammetric evolutions of the EPPGE-SWCNT-Fe_2O_3 in 0.1 M PBS solution containing different concentrations of DA (i–viii represent 0.00, 3.23, 6.25, 9.09, 11.76, 14.30, 18.92, and 31.82 µM, respectively). Inset is the plot of current vs. concentration of DA.

From the plot of current response against concentration (inset in Figure 7.7), a linear relationship (Equation 7.4) was obtained for concentration range of 0.0 to 31.8 μM.

$$I_p / \mu A = (3.44 \pm 0.03)\,[DA] / \mu M + (266.35 \pm 0.38) \qquad (7.4)$$

The sensitivity was calculated as 3.44±0.03 μA μM^{-1} (R^2 = 0.9997), while the limit of detection (LoD = 3.3 s/m [22]) was (3.6±0.3)x10^{-7} M. The limit of detection of the electrode was much lower, and at about the same magnitude with values reported in literature (Table 7.2) for some modified electrode towards DA electrocatalysis and detection [18,23,24-27]. Dopamine is present at a micromolar concentration level in biological fluids [28] thus the 3.6 x 10^{-7} M detection limit of EPPGE-SWCNT-Fe_2O_3 suggest that SWCNT/Fe_2O_3 hybrid material might be suitable for the modification of ultramicroelectrodes for in-vivo detection of dopamine.

The stability of the electrode was first interrogated by continuous scanning in a 2x10^{-4} M DA at 25 mVs^{-1}. A decrease in peak currents (>50%) was usually observed after the first scan, which is a typical behaviour for a poisoned electrode. However, on rinsing the electrode in a fresh PBS (pH 7.0) solution, the electrode surface was renewed and more than 95% of the initial catalytic current was obtained, indicating the electrochemical stability and reusability of the electrode after analysis. Also, using SWV technique, the same result as in Figure 7.7 was obtained. The electrode can be used for the analysis of DA after storage in a refrigerator for up to two weeks without a significant change in its response.

Table 7.2: Voltammetric response for dopamine using various modified electrodes.

Electrode	**Electrolyte**	**Method**	**LCR range/µM**	**LoD/ µM**	**Ref.**
EPPGE-SWCNT-Fe_2O_3	0.1 M PBS (pH 7.0)	SWV	3.2 – 31.8	0.36	This work
GCE-Poly-EBT	0.05 M PBS (pH 4.0)	DPV	0.1 – 200.0	0.02	16
CPE-Cobalt salophen	0.1 M ACS (pH 5.0)	DPV	1.0 – 100.0	0.50	20
GCE-CNT-IL gel	0.1 M PBS (pH 7.08)	DPV	1.0 – 100.0	0.10	23
GCE-polycresol red	0.1 M PBS (pH 5.0)	LSV	10.0 – 100.0	1.50	21
GCE-PEDOT-PANS	ACS (pH 5.0)	LSV	2.0 – 8.0	0.50	22
Au-Penicillamine SAM	0.1 M PBS (pH 6.8)	–	20.0 – 800.0	4.0	24

EBT: erichrome black T; CPE: carbon paste electrode; GCE: Glassy carbon electrode; CNT: Carbon nanotubes; IL: Ionic liquid; PEDOT: Poly(3,4-ethylenedioxythiophene-co-(5-amino-2-naphthalenesulfonic acid)); PANS: Poly 5-amino-2-naphthalenesulfonic acid; SAM: Self-assembled monolayer; PBS: Phosphate buffer solution; ACS: Acetate buffer solution; LCR: Linear concentration range; LoD: Limit of detection; SWV: Square wave voltammetry; DPV: Differential pulse voltammetry; LSV: Linear sweep voltammetry

Chronoamperometric study was carried out by setting the operating condition at a potential of 0.2 V. The catalytic rate constant (k) for the oxidation of DA at the EPPGE-SWCNT-Fe_2O_3 electrode was estimated from already known relationship [29,30]. From the plots of I_{cat}/I_{buff} vs. $t^{1/2}$ at different DA concentrations (not shown), and the plot of the slopes vs. square root of the DA concentrations (not shown), k value was estimated to be 8.7±0.74 x 10^5 cm^3 mol^{-1} s^{-1} for EPPGE-SWCNT-Fe_2O_3. The k value obtained in this study is *ca* 3 times higher than the 3.1 x 10^2 M^{-1} s^{-1} (3.1 x 10^5 cm^3 mol^{-1} s^{-1}) reported for DA oxidation at aluminium electrode modified with nickel pentacyanonitrosylferrate films [31], approximately 2 times higher than 4.67 x 10^2 M^{-1} s^{-1} (4.67 x 10^5 cm^3 mol^{-1} s^{-1}) reported at palladium hexacyanoferrate film, electroless plated electrode [32] and a magnitude less compared with 8.813 x 10^3 M^{-1} s^{-1} (8.813 x 10^6 cm^3 mol^{-1} s^{-1}) reported for the analyte oxidation on a modified carbon nanotube paste electrode [33]. The difference in the k value is due to the different electrode modifier. The diffusion coefficient (D) of DA at this electrode was estimated from the Cottrell Equation (7.5) below [10]:

$$I = \frac{nFAD^{1/2}C}{\pi^{1/2}t^{1/2}} \qquad (7.5)$$

where C is the bulk concentration (mol cm^{-3}), A is the area of the electrode in cm^2 and assuming n ≈ 2 [18,34,], from the experimental plots of I versus $t^{-1/2}$ at different concentrations (not shown), the diffusion coefficient D of DA was calculated as (3.5±0.27) x 10^{-5} cm^2s^{-1} for the EPPGE-SWCNT-Fe_2O_3, which closely agree with the 6.5

x 10^{-5} cm^2s^{-1} reported for *poly* (malachite green) film-coated glassy carbon electrode [21] but about a magnitude higher than 4.15 x 10^{-6} cm^2 s^{-1} reported for DA on penicillamine self-assembled gold electrode [27].

7.5. Interference study

Typical square wave voltammetric responses of AA in the absence (i) and presence of DA (ii – iv) at the EPPGE-SWCNT-Fe_2O_3 platform are shown in Figure 7.8. Curve (i) represents 1 mM AA alone, and mixture of (ii) 33.3 µM DA and 0.83 mM AA, (iii) 46.2 µM DA and 0.77 mM AA, and (iv) 88.9 µM DA and 0.56 mM AA in PBS pH 7.0. Attempts to obtain much lower concentration of the DA was not successful probably due to the base line drifts of the SWV. In the absence of DA, AA signal appeared close to zero volt. On addition of DA, there was a clear separation of signal with DA located at around 0.2 V. The height and amplitude of the peak corresponding to DA also increase proportionally with the DA concentration. It is interesting to observe that good signal of the DA at 33 µM could be obtained in the presence of 1 mM AA. In fact, in all the concentrations of the DA studied there was no detectable interference of the AA, the signal of the AA was about 200 mV away from that of the DA.

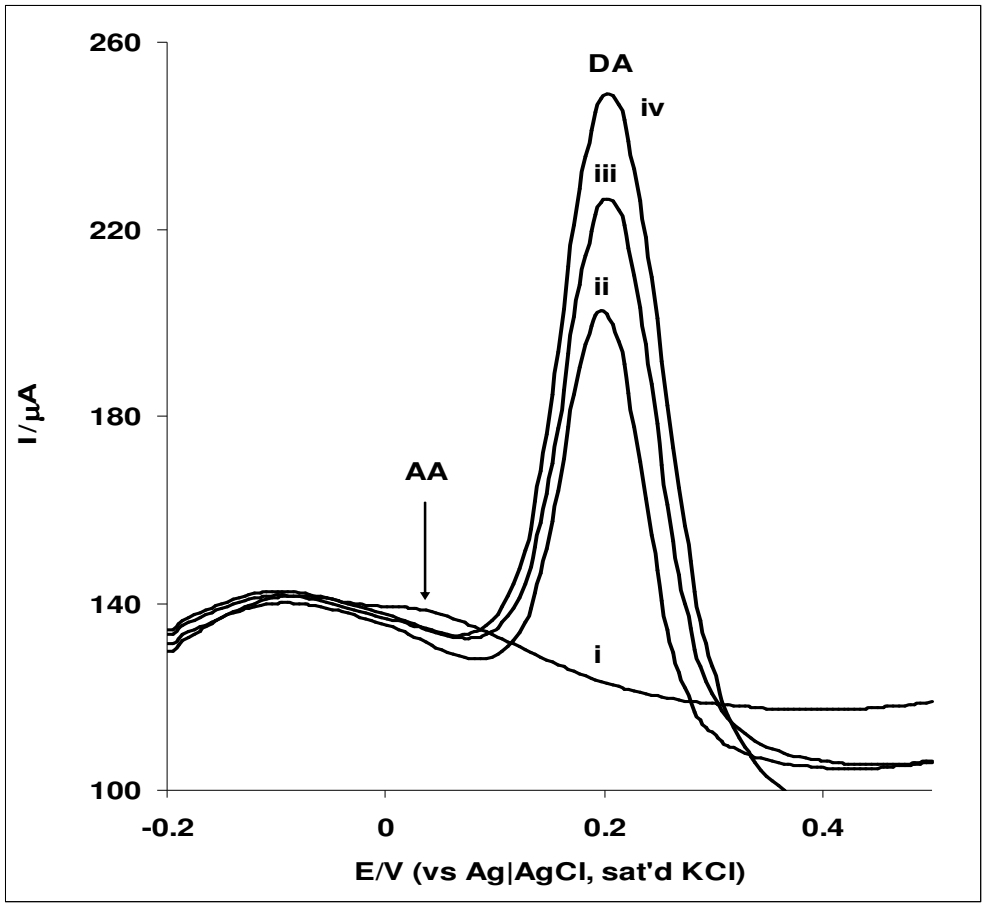

Figure 7.8: Typical square wave voltammograms responses of EPPGE-SWCNT-Fe_2O_3 in (i) 1 mM AA alone, and mixture of (ii) 33.3 µM DA /0.83 mM AA, (iii) 46.2 µM DA / 0.77 mM AA, and (iv) 88.9 µM DA / 0.56 mM AA in PBS pH 7.0.

7.6. Real sample analysis: Dopamine drug

To evaluate the potential applicability of the EPPGE-SWCNT-Fe_2O_3 electrode, a square wave voltammetric assay of dopamine present in a dopamine hydrochloride injection, with dopamine content of 200 mg / 5 mL (i.e., 40 mg mL^{-1}) was carried out. The concentration found in each dopamine drug (Table 7.3) is approximately within the labelled amount (n = 5) at 95% confidence limit. The result clearly indicates that dopamine can be reliably assayed from its drug, thus demonstrating the suitability of the proposed EPPGE-SWCNT-Fe_2O_3 electrode as a sensor.

Table 7.3: Determination of dopamine content in dopamine hydrochloride injections (40 mg mL^{-1}), n =5 (at 95% confidence limit).

Sample	Concentration found/mg mL^{-1}	Recovery/%
1	41.7 ± 2.73	104.3 ± 6.70
2	40.4 ± 0.63	101.0 ± 1.02
3	39.8 ± 0.77	99.4 ± 1.92
4	41.1 ± 0.48	102.7 ± 1.19

In a similar study, the voltammetric detection of dopamine using easily prepared nano-scaled iron oxide (Fe_2O_3) catalyst supported on multi-walled carbon nanotubes (MWCNT) modified pyrolytic graphite electrode was carried out. Some of the motivating factors for embarking on this particular study include (i) the ability to produce nano-scaled iron oxides in high commercial quantity compared to the very low and commercially unviable amount

inherent with the electrodeposition method, (ii) low or non-passivation of the electrode modified with laboratory-synthesised Fe_2O_3 nanoparticles compared with their electrodeposited counterparts, and (iii) commercial availability of MWCNTs over the SWCNTs in terms of cost implication

Figure 7.9 is the typical TEM micrograph for the MWCNT-Fe (a) and the MWCNT-Fe_2O_3 (b). Their corresponding HRSEM images are represented in Figure 7.9c and d respectively. All the micrographs showed very high dispersion of Fe and Fe_2O_3 nanoparticles along the MWCNTs which is made possible because of the strong electrostatic interactions between the Fe^{2+} or Fe^{2+} ions in solution and the COO^- charge of the MWCNTs. From the TEM and using the UTHSCSA Image Tool for windows version 3.0, for the image calibration, a representative single particle size is around 20-50 nm for Fe and 5-13 nm for Fe_2O_3 which agreed closely with 60-70 nm reported for Fe [35], and 8.6 nm for γ-Fe_2O_3 nanoparticles [36].

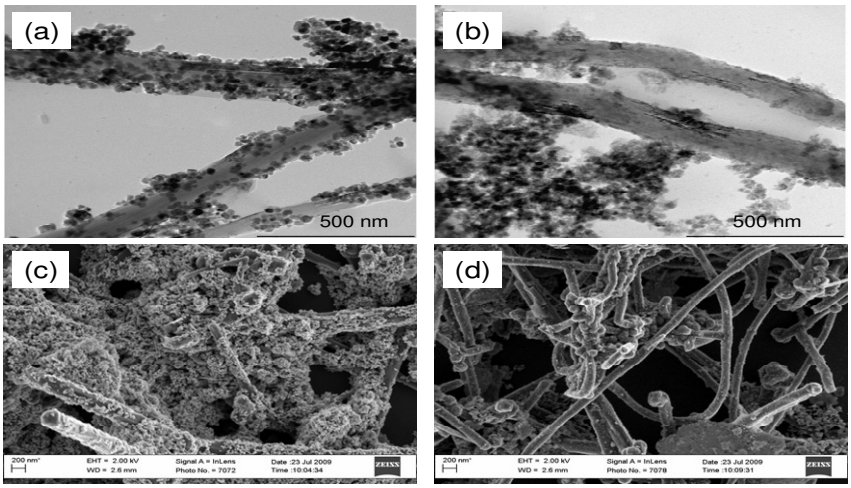

Figure 7.9: TEM images of (a) MWCNT-Fe (b) MWCNT-Fe_2O_3. (c) and (d) HRSEM picture of MWCNT-Fe and MWCNT-Fe_2O_3 respectively.

The XRD spectra for the nanosized particles are shown in Figure 7.10. Characteristic peaks at 2θ of 21.3, 35.2, 41.5, 50.6, 62.6, 67.4 and 74.3, which are indexed as (111), (220), (311), (400), (422), (511) and (440) were observed. The result agreed with that observed by others [36,37] indicating that the resultant particles were cubic spinel structure for γ-Fe_2O_3. From Debye-Scherrer equation [36], the crystal size of the Fe_2O_3 particles were estimated from the peaks to be ~ 10.3 nm, which falls in the range shown by the TEM. Inset in Figure 7.10 is the XRD spectrum of the Fe nanoparticles. Apparent peaks at 2θ of 41.8 and 35.4 indicate the presence of both zero-valent iron (Fe) and iron oxide (FeO) [35]. Traces of FeO particles not completely reduced to Fe were also confirmed by the presence of trace oxygen peak in the EDX profile (see Figure 7.11a).

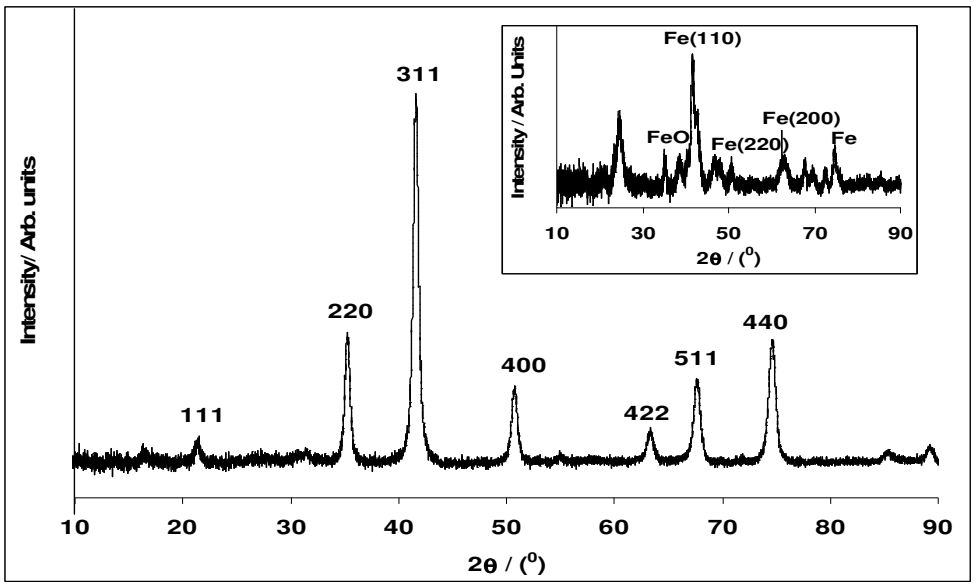

Figure 7.10: XRD spectrum of Fe_2O_3 nanoparticles. Inset is the XRD spectrum of Fe nanoparticles.

Figure 7.11 shows the EDX profile of the synthesised MWCNT-Fe (a) and MWCNT-Fe_2O_3 (b). The carbon peak in both is attributed to the carbon of the MWCNT or the base carbon coating for enhancing the conductivity of the material. The presence of Fe peaks in both (a) and (b) compared with other elements also confirm the successful modification of the MWCNTs with Fe or Fe_2O_3 nanoparticles. Presence of O peak in (b) is linked to traces of unreduced iron oxide and the oxo-functionalities of the functionalised MWCNTs. The sulphur peak can be attributed to the sulphuric acid used during MWCNT treatment.

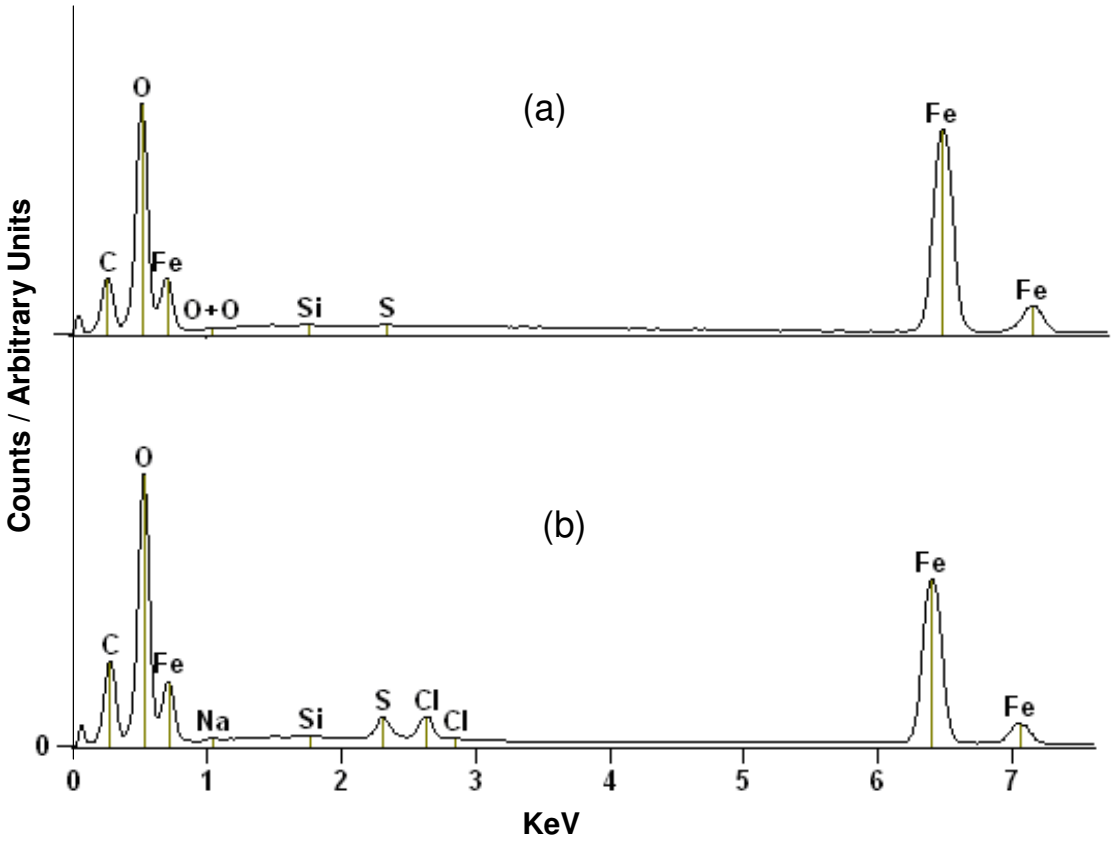

Figure 7.11: EDX profiles of MWCNT-Fe and MWCNT-Fe_2O_3 respectively.

Figure 7.12(a) is the comparative cyclic voltammograms of the electodes in 5 mM $Fe(CN)_6]^{4-}/[Fe(CN)_6]^{3-}$ solution. The redox couple in the 0.0 – 0.4 V regions (II) is due to the $Fe(CN)_6]^{4-}/[Fe(CN)_6]^{3-}$ redox process. This couple is absent in 0.1 M PBS (pH 7) alone (b). The broad redox process in the -0.2 – 0.2 V region (I) is ascribed to the Fe^{3+}/Fe^{2+} of the iron or iron oxide, presumably the γ-Fe_2O_3 / Fe_3O_4. The poorly defined redox couples in the 0.5 – 0.7 V (III) is presumably due to the redox process involving the α-phase (i.e., α-Fe_2O_3 / FeOOH).

Further study to understand the electronic transport properties of the modified electrodes was carried out using electrochemical impedance spectroscopic (EIS) technique (biased at 0.2 V, the equilibrium potential, $E_{1/2}$, of the $[Fe(CN)_6]^{4-}/[Fe(CN)_6]^{3-}$ couple). The Nyquist plot obtained (Figure 7.13a) was satisfactorily fitted using the electrical equivalent circuit model shown in Figure 7.13b. The circuit elements are already defined. From the R_{ct} value (Table 7.4), the electron-transport is faster at the EPPGE-MWCNT-Fe and EPPGE-MWCNT-Fe_2O_3 electrodes (R_{ct} ~ 20.0 Ωcm^2) compared to others. The n values close to the ideal Warburg diffusive value of 0.5, is indicative of some diffusion process at the electrode.

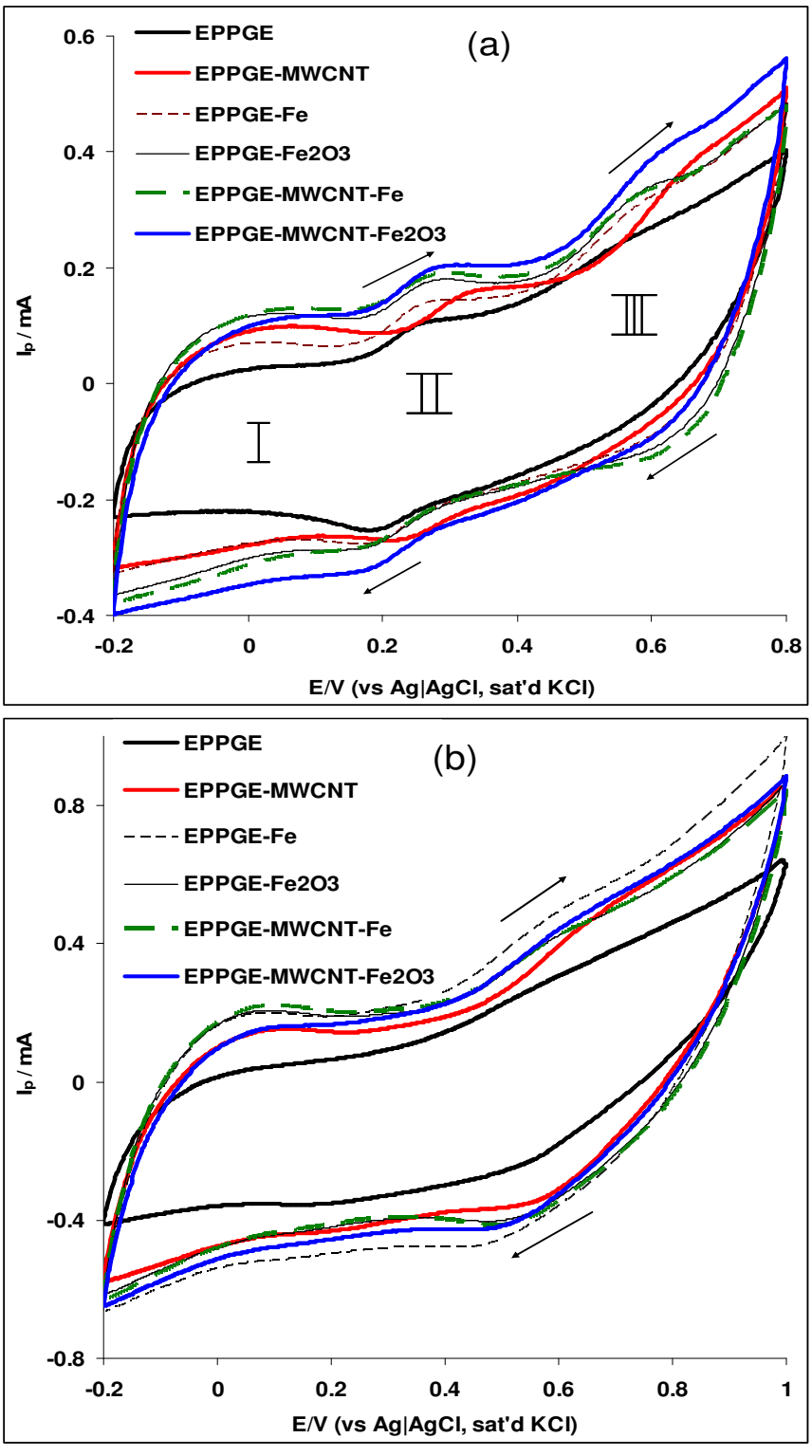

Figure 7.12: Comparative cyclic voltammetric evolutions of the bare and Fe/Fe_2O_3 modified electrodes in (a) 5 mM $[Fe(CN)_6]^{4-}/[Fe(CN)_6]^{3-}$ in pH 7.0 PBS and (b) 0.1 M pH 7.0 PBS (scan rate = 50 mVs^{-1}).

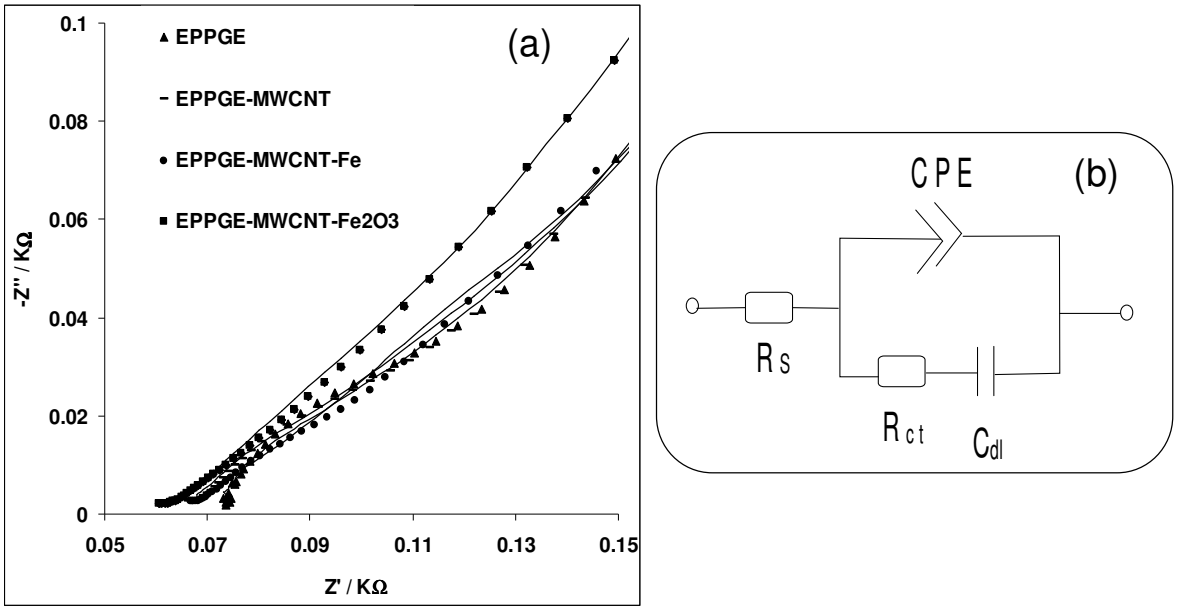

Figure 7.13: (a) Typical Nyquist plots obtained for some of the MWCNT modified electrodes in 5 mM $[Fe(CN)_6]^{4-}$ / $[Fe(CN)_6]^{3-}$ solution at a fixed potential of 0.2 V (vs Ag|AgCl, sat'd KCl). (b) is the circuit used in the fitting of the EIS data in (a).

Table 7.4: Impedance data obtained for the bare and the MWCNT modified EPPGE electrodes in 5 mM $Fe(CN)_6]^{4-}/[Fe(CN)_6]^{3-}$ solution at 0.2 V (vs Ag|AgCl sat'd KCl).

Electrodes	**Impedimetric parameters**				
	R/Ωcm^2	**Q/μFcm^{-2}**	**N**	**R/Ωcm^2**	**C_{dl}/mFcm^{-2}**
EPPGE	6.96±0.01	14.0±1.24	0.51±0.01	35.00±0.19	1.28±0.06
EPPGE-MWCNT	6.46±0.01	11.3±1.16	0.49±0.01	35.30±0.20	1.72±0.08
EPPGE-Fe	3.14±0.01	10.8±1.01	0.47±0.01	24.15±0.13	3.10±0.15
EPPGE-Fe_2O_3	3.29±0.01	161.8±19.61	0.55±0.01	27.10±0.69	1.15±0.22
EPPGE-MWCNT-Fe	3.33±0.01	38.0±4.74	0.49±0.01	20.2±0.18	3.94±0.30
EPPGE-MWCNT-Fe_2O_3	3.08±0.01	91.8±8.18	0.52±0.01	19.75±2.05	2.78±0.23

Figure 7.14 is the comparative cyclic voltammograms of the electrodes in 0.1 M PBS containing $2x10^{-4}$ M dopamine (DA). DA catalysis was studied at different loading (2.5 – 10 mg mL^{-1}) of Fe and Fe_2O_3 nanoparticles or their nanocomposite with MWCNT on the electrode. Since Fe, Fe_2O_3 and the MWCNTs are characterised with background (or capacitive) current, the current due to dopamine electro-oxidation (*ca* 0.2 V) on the electrodes was obtained after the background subtraction. Interestingly, when compared with all known literature reports on dopamine oxidation at modified electrodes, this result represents the first time that two pairs of redox couples are observed for dopamine. From the preceding discussion, the first DA redox couple (Dopamine / Quinone) at $E_{1/2}$ of 0.16 V is the usual mediated by the Fe^{3+}/Fe^{2+} (i.e., the γ-Fe_2O_3 / Fe_3O_4). The second redox couple at $E_{1/2}$ of 0.40 V is the same Dopamine / Quinone, which is now presumably mediated by the α-phase (i.e., α-Fe_2O_3 / FeOOH). The highest DA signal was obtained at 5.0 $mgmL^{-1}$ loading of the nanocomposite on the electrode and the trend in current response follows as: MWCNT-Fe_2O_3 >> MWCNT-Fe > MWCNT > EPPGE ≈ Fe_2O_3 > Fe. The current response at the MWCNT-Fe_2O_3 electrode is about two times higher than that at the bare electrode as well as the electrodes based on MWCNT or Fe nanoparticles alone. The DA oxidation current decreased with increasing loading (7.5 to 10 $mgmL^{-1}$) of the nanocomposite suggesting electrode layer passivation. The enhanced DA response at EPPGE-MWCNT-Fe_2O_3 may be ascribed to either (1) facile interaction of MWCNTs and Fe_2O_3, or (2) the ease of diffusion of DA through the MWCNT-Fe_2O_3 film to the electrode surface, or (3) the ability of the iron (III) to forms a chelate with the dihydroxy catechol group of dopamine, catechol, 5, 6-dihydroxyindole [38], or all of them. The

DA current response at the MWCNT-Fe_2O_3 films modified electrode is also higher compared with 50.45 µA reported for the SWCNT-Fe_2O_3 electrode prepared by electrodeposition method. The result therefore suggest that the synthetic method adopted in this study could be a better approach for electrode modification with the nanocomposite materials in large quantity, and at lesser cost for commercial application in sensor and other electrochemical devices. Therefore, all other studies carried out in this work, unless otherwise stated, were carried out using EPPGE-MWCNT-Fe_2O_3 electrode.

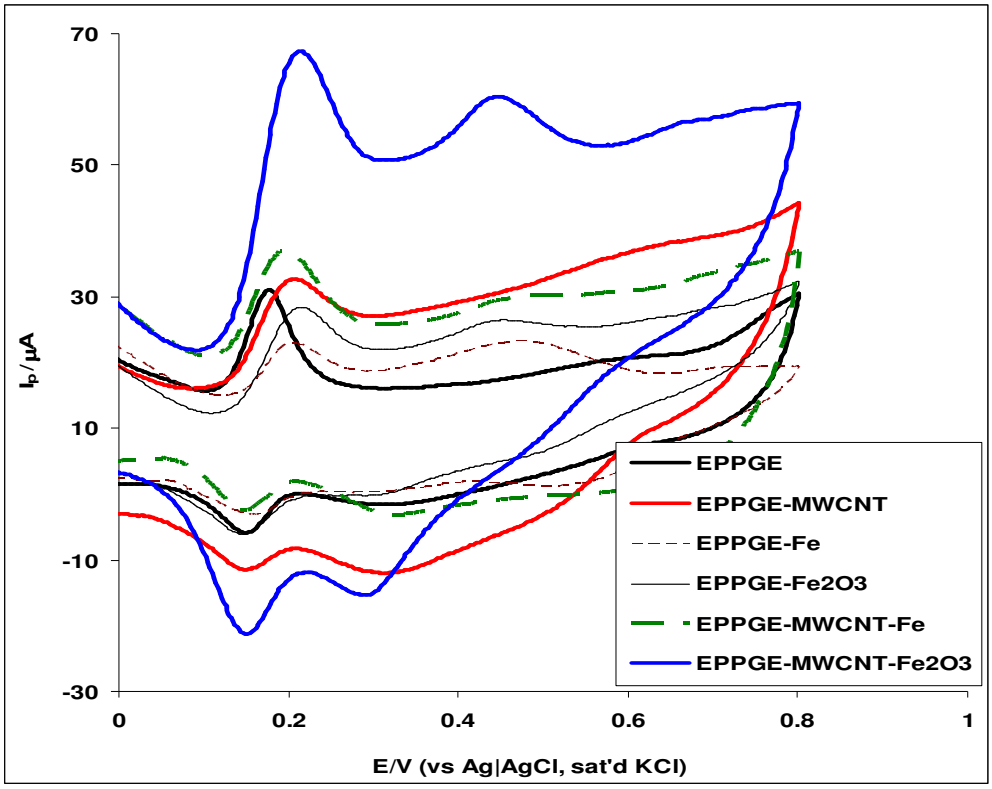

Figure 7.14: Comparative current response (after background current subtraction) of the electrodes: (i) EPPGE, (ii) EPPGE-MWCNT, (iii) EPPGE-Fe, (iv) EPPGE-Fe_2O_3, (v) EPPGE-MWCNT-Fe, and (vi) EPPGE-MWCNT-Fe_2O_3 in $2x10^{-4}$ M DA solution in pH 7.0 PBS (scan rate = 25 mVs^{-1}).

Effect of scan rate (ν) was investigated by carrying out cyclic voltammetry experiment at constant concentration (2 x 10^{-4} M) of DA in 0.1 M PBS using the EPPGE-MWCNT-Fe_2O_3 electrode (Figure 7.15). It was observed that DA anodic and cathodic peaks increase simultaneously with increase in scan rates (25–1000 mV s^{-1}). A pair of well defined symmetrical redox peaks (I_{pa} /I_{pc} ~ 1.0), were observed even at high scan rates. However, plots of the anodic (I_{pa}) against the square root of scan rate ($\nu^{1/2}$) (not shown) for the scan rate range studied gave a linear relationship with scan rates (R^2 = 0.9932), suggesting a diffusion-controlled redox process.

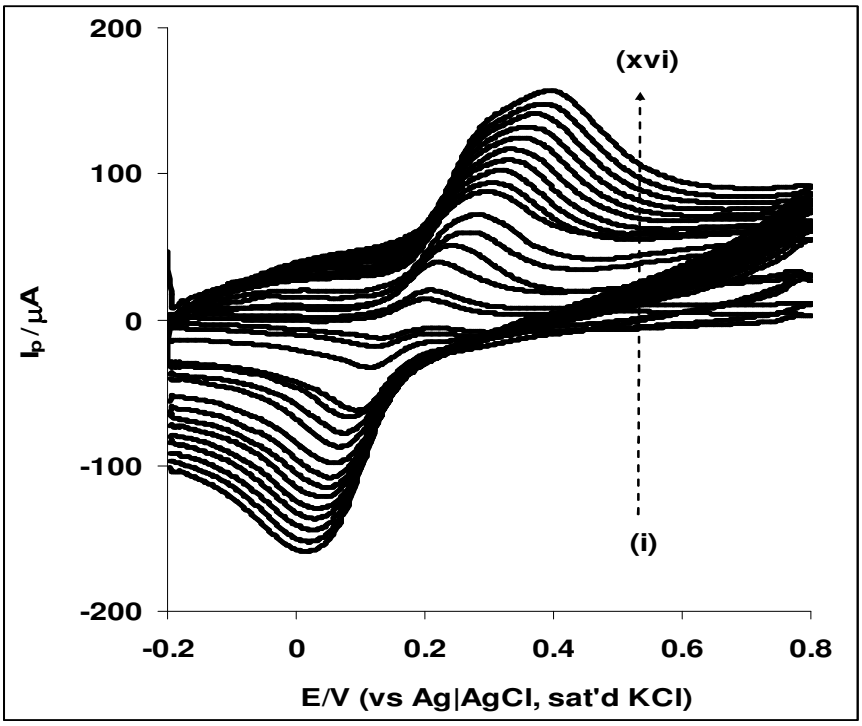

Figure 7.15: Cyclic voltammetric evolutions of EPPGE-MWCNT-Fe_2O_3 obtained in 0.1 M PBS containing 2 x 10^{-4} M DA (scan rate range 25 – 1000 mVs^{-1}; inner to outer).

Electro-oxidation of DA at the electrodes was investigated using EIS at a fixed potential (0.2 V vs. Ag|AgCl, sat'd KCl) and frequency range of 10 kHz to 10 mHz. Figure 7.16 represents the Nyquist plots obtained for some of the electrodes. Inset is the modified Randles circuit model used in the fitting of the experimental data. The circuit elements are already defined. The R_{ct} value (31.6 Ωcm^2) for EPPGE-MWCNT-Fe_2O_3 is relatively low compared with the 33.4 Ωcm^2 for bare EPPGE and 38.9 Ωcm^2 for EPPGE-MWCNT (Table 7.5). The results demonstrated the role of the MWCNT in forming a synergy with the Fe_2O_3 nanoparticles in improving the catalysis and electron transport of the MWCNT-Fe_2O_3 electrode towards DA oxidation. Presently, there is very little information on DA electrochemical impedance study. The information using a fibre (SiC-C) electrode for DA sensing [34] indicated that the electrode showed a capacitive behaviour which, according to the authors, is highly desirable for chemical and electrochemical stability of the electrodes.

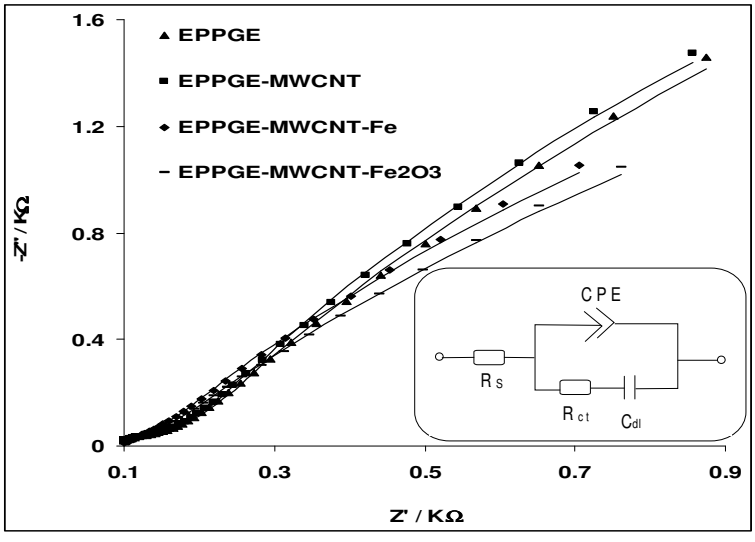

Figure 7.16: Typical Nyquist plots obtained for some of the MWCNT modified electrodes in 2 x 10^{-4} M DA solution at a fixed potential of 0.2 V. Inset is the Randles circuit model used in fitting the data.

Table 7.5: Impedance data obtained for the bare and the modified EPPGE electrodes in 2 x 10^{-4} M DA in pH 7.0 PBS at 0.2 V (vs Ag|AgCl sat'd KCl).

Electrodes	**Impedimetric parameters**				
	$R_s/\Omega cm^2$	**$Q/\mu Fcm^{-2}$**	**N**	**$R_{ct}/\Omega cm^2$**	**$C/mFcm^{-2}$**
EPPGE	8.32±0.01	24.19±2.15	0.57±0.01	33.40±0.13	2.20±0.05
EPPGE-MWCNT	8.30±0.01	25.06±2.09	0.58±0.01	38.90±0.16	2.19±0.08
EPPGE-Fe	8.71±0.01	12.39±1.27	0.53±0.01	40.30±0.17	2.40±0.09
EPPGE-Fe_2O_3	8.71±0.01	96.23±4.86	0.61±0.01	57.50±0.36	1.40±0.07
EPPGE-MWCNT-Fe	8.77±0.01	133.50±12.88	0.62±0.01	30.85±0.31	1.67±0.12
EPPGE-MWCNT-Fe_2O_3	8.42±0.01	83.06±4.86	0.59±0.01	31.60±0.21	1.46±0.07

The stability of the electrode was studied by continuous scanning in 2×10^{-4} M DA at 25 mVs^{-1}. About 40% current decrease was observed after the first scan which could be due to the adsorbed species on the electrode. However, on rinsing the electrode in a fresh PBS (pH 7.0) solution, the electrode surface became renewed and a current increase (> 90%) of the initial catalytic current was obtained. The result therefore suggests that the electrode is electrochemically stable and can be reused after an experiment. The electrode also demonstrated an insignificant change to DA current response during DA analysis after storage in a refrigerator for up to two weeks.

Concentration study was carried out by investigating the response of EPPGE-MWCNT-Fe_2O_3 electrode to the different concentrations of DA (Figure 7.17) using square wave voltammetry (SWV) experiments at a fixed potential of 0.20 V. From the plot of current response against concentration (not shown), a linear relationship was obtained for concentration range of 6.3 to 25.0 µM. The sensitivity was calculated as 0.026±0.002 $\mu A \mu M^{-1}$, while the limit of detection (LoD = 3.3 s/m) was (3.3±0.28) x 10^{-7} M. The limit of detection obtained in this study agreed closely with the 0.36 µM reported for EPPGE-SWCNT-Fe_2O_3 using same technique but much lower, or at about the same magnitude with values reported in literature for DA electro-oxidation [24,26,29,39-43]. The catalytic rate constant (k) for the oxidation of DA at the EPPGE-SWCNT-Fe_2O_3 electrode was estimated using chronoamperomatric technique and a known relationship [29,30,44]. From the slope of the plots of I_{cat}/I_{buff} vs. $t^{1/2}$ at different DA concentrations (not shown), the k value was estimated as (16.4±1.48) x 10^5 $cm^3mol^{-1}s^{-1}$.

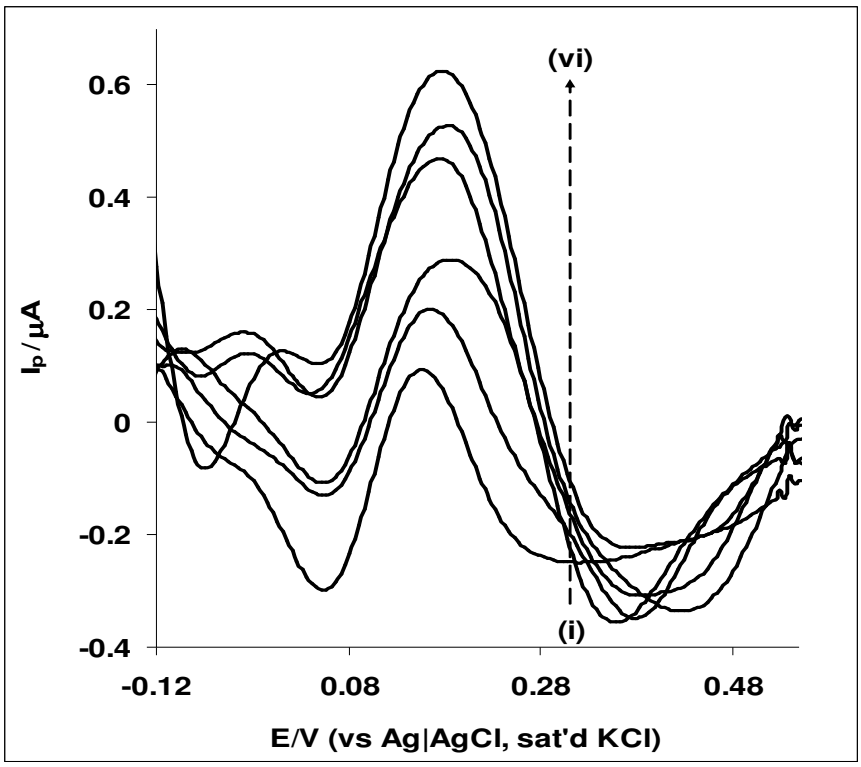

Figure 7.17: Square wave voltammetric evolutions of the EPPGE-MWCNT-Fe_2O_3 in 0.1 M PBS pH 7.0 containing different concentration of DA (6.25, 11.8, 14.7, 21.1, 23.1 and 27.0 µM).

The *k* value is greater compared with 4.67 x 10^5 cm^3 $mol^{-1}s^{-1}$ reported for DA on aluminium electrode modified with palladium hexacyanoferate (PdHCF) films [32] and 3.1 x 10^5 $cm^3mol^{-1}s^{-1}$ on aluminium electrode modified with nickel pentacyanonitrosylferrate (NiPCNF) film [33]. The diffusion coefficient *D* for DA at the electrode was estimated from Equation 7.5 above. The diffusion coefficient *D* for DA was calculated as (8.4±0.67) x 10^{-5} cm^2s^{-1}. The *D* value is a magnitude higher than the 2.5 x 10^{-6} cm^2s^{-1} reported for DA on aluminium electrode modified with palladium hexacyanoferate (PdHCF) films [32], and 3.4 x 10^{-6} cm^2s^{-1} for DA on aluminium electrode modified with nickel pentacyanonitrosylferrate (NiPCNF)

film [33]. The difference in *K* and *D* reported for the electrodes is due to their different surface electroactive materials.

Figure 7.18 shows the square wave voltammetric responses of AA in the absence (1 mM AA alone) (i), and mixture of (ii) 4.76 µM DA and 0.95 mM AA, (iii) 9.09 µM DA and 0.91 mM AA, (iv) 13.04 µM DA and 0.87 mM AA, (v) 20.0 µM DA and 0.8 mM AA, (vi) 25.93 µM DA and 0.74 mM AA and (vii) 28.57 µM DA and 0.71 mM AA in PBS pH 7.0 at the EPPGE-MWCNT-Fe_2O_3 electrode. In the presence of DA, AA signal was seen at about 0.18 V and DA at around 0.37 V on the electrode, which is contrary to AA and DA position observed at *ca* 0.1 and 0.2 V respectively on EPPGE-SWCNT-Fe_2O_3 electrode made by electrodeposition. Cao et al. [45] also observed AA and DA signal at 0.14 and 0.43 V respectively on CPB/chitosan composite films modified glassy carbon electrode. In this study, the potential difference of 190 mV between the two analytes is large enough for the determination of one in the presence of the other. However, the electrode appeared weak towards AA detection thus enhancing a negative shift (about 170 mV) in DA signal, with increasing DA current as DA concentration increases (ii-vii) while AA peaks disappeared completely. The implication of this result is that, there is no possible fouling effect due to AA oxidation intermediates, and the EPPGE-MWCNT-Fe_2O_3 electrode attracted DA strongly leading to enhanced catalysis and fast electron transport towards DA oxidation.

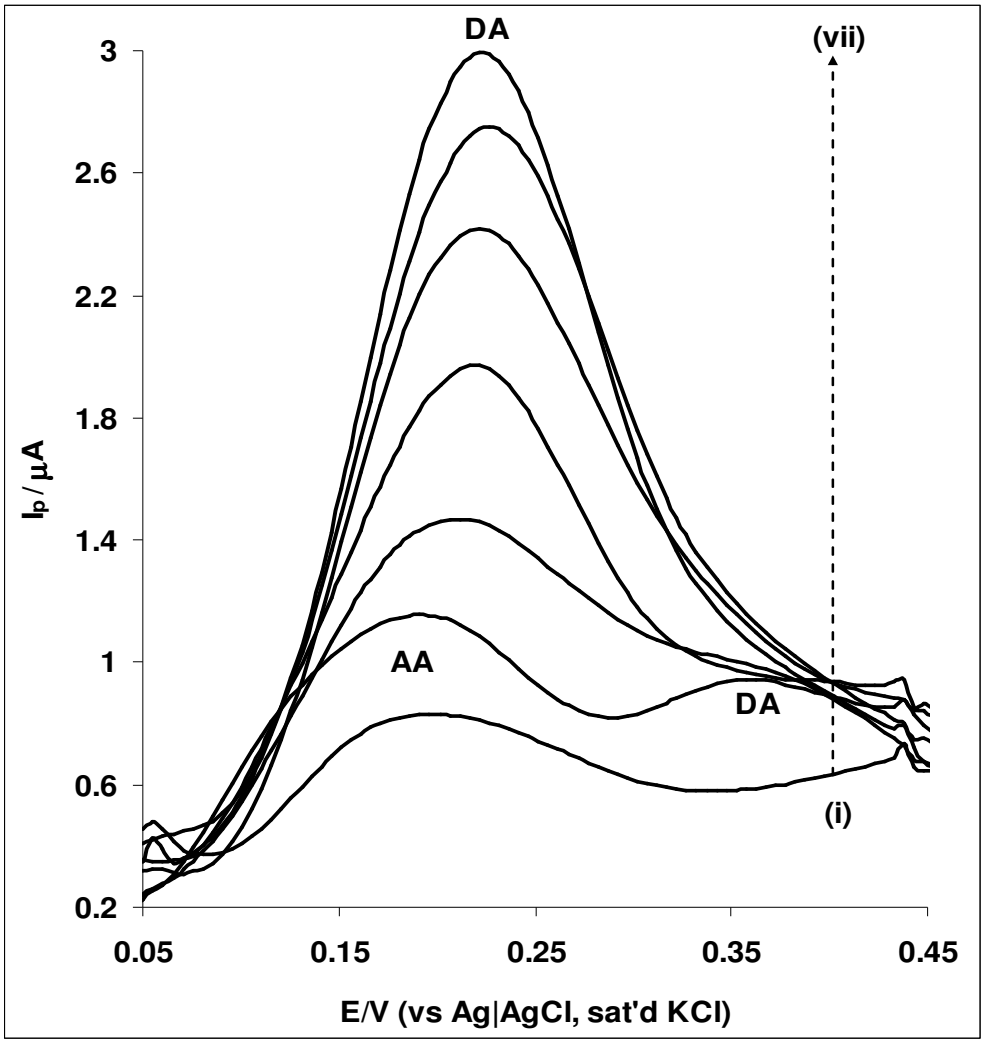

Figure 7.18: Typical square wave voltammograms responses of EPPGE-MWCNT-Fe_2O_3 in (i) 1 mM AA alone, and mixture of (ii) 4.76 µM DA and 0.95 mM AA, (iii) 9.09 µM DA and 0.91 mM AA, (iv) 13.04 µM DA and 0.87 mM AA, (v) 20.0 µM DA and 0.8 mM AA, (vi) 25.93 µM DA and 0.74 mM AA, and (vii) 28.57 µM DA and 0.71 mM AA in PBS pH 7.0.

The potential applicability of the EPPGE-MWCNT-Fe_2O_3 electrode was tested with a square wave voltammetric assay of dopamine present in a dopamine hydrochloride injection (dopamine content of 200 mg / 5 mL or 40 mg / mL). The concentration found in each dopamine drug (Table 7.6) agreed closely with the labelled amount, with average recovery (n=5) of 100.6±2.37% at 95%

confidence limit. The result proves the suitability of the EPPGE-MWCNT-Fe_2O_3 electrode for DA detection in biological samples.

Table 7.6: Determination of dopamine content in dopamine hydrochloride injections (40 mg mL^{-1}), n =5 (at 95% confidence limit) using EPPGE-MWCNT-Fe_2O_3 electrode.

Sample	Concentration found/mg mL^{-1}	Recovery/%
1	40.6 ± 0.52	101.5 ± 1.30
3	39.9 ± 1.01	99.8 ± 2.53
4	39.5± 0.96	98.7 ± 2.38
2	40.9 ± 1.24	102.2 ± 3.09

This study describes the efficient electrocatalytic detection of DA using electrodeposited Fe_2O_3 nanoparticle catalyst supported on a SWCNT-modified edge-plane pyrolytic graphite electrode (EPPGE) platform (EPPGE-SWCNT-Fe_2O_3). The SWCNT-Fe_2O_3 nanoparticles enhanced the electrocatalytic response towards the detection of DA, in terms of peak current compared to other electrodes investigated. Electron transfer properties and electrocatalytic behaviour towards the detection of dopamine using iron oxide nanoparticle (γ-Fe_2O_3) catalysts supported on MWCNTs was also carried out. It was shown that these synthesized γ-Fe_2O_3 nanoparticles exhibit comparable electrocatalytic behaviour with their electrodeposited forms, but uniquely different in terms of the electrochemical properties. From EIS, the pseudo-capacitive nature of the modified EPPGE electrodes is a function of their electrochemical stability towards DA. Analysis of DA at both the EPPGE-SWCNT-Fe_2O_3 and the EPPGE-MWCNT-Fe_2O_3

electrodes showed that DA oxidation proceeded through diffusion and surface controlled electrochemical process. The limit of detection, catalytic rate constant of the electrodes, and the diffusion coefficient of DA agreed favourably with values reported earlier in literature. The modified SWCNT-Fe_2O_3 /MWCNT-Fe_2O_3 electrodes clearly separated DA signal from the interfering effect of AA even at AA concentration which is 50-100 folds that of DA. The electrode had also proven to be a potential sensor for dopamine detection in real drug analysis.

References

1. N. S. McIntyre, M. G. Cook, *Anal. Chem.* 47 (1975) 2208.

2. Sunohara, K. Nishimura, K. Yahikozawa, M. Ueno, M. Enyo, Y. Takasu, *J. Electroanal. Chem.* 354 (1993) 161.

3. M. Aronniemi, J. Sainio, J. Lahtinen, *Appl. Surf. Sci.* 253 (2007) 9476.
4. H. Luo, Z. Shi, N. Li, Z. Gu, Q. Zhuang, *Anal. Chem.* 73 (2001) 915.

5. I.D. Raistrick, D.R. Franceschetti, J.R. Macdonald, In: *Impedance Spectroscopy: Theory Experiment, and Applications*, 2nd ed, E. Barsoukov and J.R. Macdonald (eds.), Wiley, Hoboken, New Jersey, 2005, Chap. 2, pp.27-128.

6. X. Wu, H. Ma, S. Chen, Z. Xu, A. Sui*, J. Electrochem. Soc.* 146 (1999)1847.

7. G. Nurk, H. Kasuk, K. Lust, A.E. Janes, *J. Electroanal. Chem.* 553 (2003) 1.
8. M.E. Orazem, B. Tribollet, *Electrochemical Impedance Spectroscopy*, John Wiley & Sons Inc, Hoboken, NJ., 2008, (ch. 13).

9. A.T. Chidembo, K.I. Ozoemena, B.O. Agboola, V. Gupta, G.G. Wildgoose, R.G. Compton, *Energy Environ. Sci.* 3 (2010) 228.

10. A.J. Bard, L.R. Faulkner, *Electrochemical. Methods: Fundamentals and Applications*, 2nd Ed, John Wiley & Sons, 2001, Hoboken NJ.
11. H.H. Girault, *Analytical and Physical Electrochemistry*, EPFL Press, Lausanne, Switzerland, 2004, (ch. 7).

12. K.I. Ozoemena, D. Nkosi, J. Pillay, *Electrochim. Acta* 53 (2008) 2844.

13. H. R. Zare, N. Nasirizadeh, F. Chatraei, S. Makarem, *Electrochim. Acta* 54 (2009) 2828.
14. L.K. Charkoudian, K.J. Franz, *Inorg. Biochem.* 45 (2006) 3657.

15. M.J. Giz, B. Duong, N.J. Tao, *J. Electroanal. Chem.* 465 (1999) 72.
16. J. Wang, Y. Wang, H. Lv, F. Hui, Y. Ma, S. Lu, Q. Sha, E. Wang, *J. of Electroanal. Chem.* 594 (2006) 59.

17. S. Shahrokhian, S. Bozorgzadeh, *Electrochim. Acta* 51 (2006) 4271.
18. S. Majdi, A. Jabbari, H. Heli, A.A. Moosavi-Movahedi, *Electrochim. Acta* 52 (2007) 4622.

19. H. Yao, Y. Sun, X. Lin, Y. Tang, L. Huang, *Electrochim. Acta* 52 (2007) 6165.
20. S. Jo, H. Jeong, S.R. Bae, S. Jeon, *Microchem. Journ.* 88 (2008) 1.

21. X. Wang, N. Yang, Q. Wan, X. Wang, *Sens. Actuators B Chem.* 128 (2007) 83.

22. G. D. Christian, *Analytical Chemistry*, 6th ed. John Wiley and Sons New York, 2004, p 113.
23. Y. F Zhao, Y. Q. Gao, D. P. Zhan, H. Liu, Q. Zhao, Y. Kou, Y. H. Shao, M. X. Li, Q. K.; Zhuang, Z. W. Zhu, *Talanta* 66 (2005) 51.

24. S. Shahrokhian, H. R. Zare-Mehrjardi, *Sens. Actuators B Chem.* 121 (2007) 530.

25. W. Chen, X. Lin, L. Huang, H. Luo, *Microchim. Acta* 151 (2005) 101.
26. A. Balamurugan, S. Chen, *Anal. Chim. Acta* 596 (2007) 92.

27. Q. Wang, D. Dong, N. Li, *Bioelectrochem.* 54 (2001) 169.

28. T. Selvaraju, R. Ramaraj, *J. Electroanal. Chem.* 585 (2005) 290.

29. M. H. Pournaghi-Azar, R. Sabzi, *J. Electroanal. Chem.* 543 (2003) 115.
30. K. M. Manesh, P. Santosh, A. I. Gopalan, K. P. Lee, Enhanced *Electroanalysis* 18 (2006) 894.

31. H. Razmi, M. Agazadeh, B. Habibi-A, *J. Electroanal. Chem.* 547 (2003) 25.

32. H. Razimi, A. Azadbakht, *Electrochim. Acta* 50 (2005) 2193.

33. M. Mazloum-Ardakani, H. Beitollahi, B. Ganjipour, H. Naeimi, M. Nejati, *Bioelectrochem.* 75 (2009) 1.

34. S. Singh, R. C. Buchanan, SiC-C fiber electrode for biological sensing, *Mat. Sc. Engnr. C.* 27 (2007) 551.
35. Y-P. Sun, X-q. Li, J. Cao, W-x. Zang, H. P. Wang, *Advances in Colloid and Interface Science* 120 (2006) 47.

36. Y-K. Sun, M. Ma, Y. Zhang, N. Gu, *Colloids and Surfaces A: Physicochem.Eng.Aspects* 245 (2004) 15.

37. G. Carja, Y. Kameshima, K. Okada, *Microporous and Mesoporous Materials* 115 (2008) 541.

38. K.L. Double, L. Zecca, P. Costi, M. Mauer, C. Griesinger, S. Ito, D. Ben-shachar, G. Bringmann, R.G. Fariello, P. Riederer, M. Gerlach, *J. Neurochem*. 75 (2000) 2583.

39. B.N. Chandrashekar1, B.E. Kumara Swamy, M. Pandurangachar, S.S Shankar1, O. Gilbert1, J.G. Manjunatha, B.S., Sherigara, *Int. J. Electrochem. Sci.* 5 (2010) 578.

40. S.S Shankar, B.E.K. Swamy, M. Pandurangachar, U. Chandra1, B.N. Chandrashekar, J.G. Manjunatha, B.S. Sherigara, *Int. J. Electrochem. Sci.* 5 (2010) 944.

41. G. Alarco´n-Angeles, B. Pe´rez-Lo´pez, M. Palomar-Pardave, M.T. Ramı´rez-Silva, S. Alegret, A. Merkoci, *Carbon* 46 (2008) 898.
42. M. Pandurangachar1, B.E.K. Swamy, B.N. Chandrashekar, O. Gilbert, S. Reddy, B.S. Sherigara, *Int. J. Electrochem. Sci.* 5 (2010) 1187.

43. M.T. Shreenivas1, B.E.K. Swamy, U. Chandra, S.S. Shankar, J.G. Manjunatha, B.S. Sherigara, *Int. J. Electrochem. Sci.* 5 (2010) 774.
44. Z. Galus, Fundamentals of Electrochemical Analysis, Ellis Horwood Press, New York, 1976, p. 313, Ch. 10.
45. X. Cao, L. Luo, Y. Ding, X. Zou, R. Bian, *Sens. Actuat. B Chem.* 129 (2008) 941.